



Synthesis and characterization of niobium carbide thin films on diamond surface for superconductive application

R.A. Khmelnitsky^{a,b}, V.P. Martovitsky^a, J.V. Bondareva^{c,*}, A.I. Kolbatova^d, N.A. Titova^d, G.N. Goltsman^{d,e}, F.S. Fedorov^c, A.V. Egorov^c, N.A. Matsokin^c, A.G. Kvashnin^c, D.G. Kvashnin^f, S.A. Evlashin^c

^a Lebedev Physical Institute, Russian Academy of Sciences, 53 Leninsky Prospect, Moscow 119991, Russian Federation

^b Kotelnikov Institute of Radio Engineering and Electronics, Russian Academy of Sciences, Moscow region, Fryazino 141190, Russian Federation

^c Skolkovo Institute of Science and Technology, 30, bld. 1 Bolshoy Boulevard, Moscow 121205, Russian Federation

^d Moscow Pedagogical State University, 29 Malaya Pirogovskaya Street, Moscow 119992, Russian Federation

^e National Research University Higher School of Economics, 20 Myasnitskaya Street, Moscow 119992, Russian Federation

^f Emanuel Institute of Biochemical Physics of the Russian Academy of Sciences, 4 Kosigina st., Moscow 119334, Russian Federation

ARTICLE INFO

Keywords:

Niobium carbide
Thin films
Superconductivity
Diamond metallization

ABSTRACT

Diamond's unique properties make it attractive for use in a variety of industrial applications. However, this material has not found mass application in microelectronics due to several factors, including the lack of large-sized plates, n-type doping, and high-quality metallization. In this article, we address the problem of diamond surface metallization by forming niobium carbide layers. We obtained a niobium carbide film several nanometers thick that exhibits superconducting behavior up to 12.4 K. To our knowledge, this is the highest superconducting transition temperature achieved in the niobium carbide system. The crystal lattice parameter of the film is 4.4659 Å, which is close to the maximum value for niobium carbide lattice parameters. Density functional theory calculations were employed to investigate the thermodynamic stability of niobium carbide compounds at various temperatures and determine the superconducting critical temperature of niobium carbide. The combination of diamond's high thermal conductivity, along with the strong adhesion and superconductivity of niobium carbide films, introduces exciting possibilities for the realization of superconductive sensitive detectors.

1. Introduction

Beautiful shape, transparency and high brightness of diamond has long attracted jewelry lovers, but in addition to the visual characteristics diamond has outstanding material properties interesting in terms of industrial applications of diamond in optics, electronics, electrochemistry and thermal control [1–5]. One of the important practical issues on the way to implementing high-power applications is diamond metallization, which involves depositing a thin layer of transition metal on a diamond matrix with good adhesion [6]. Diamond metallization is used to improve its original physical properties [7] and to impart new characteristics to the diamond surface, such as excellent thermal conductivity [8], thermal stability [9], and wettability for metal or alloy dissolution. Due to the chemical inertness of diamond, the one effective method of adhesive diamond metallization is its sintering with metals such as Ti, Cr, Si, Nb, Ta, Zr, V, Hf, Mo, W, etc. [10,11], which in

reaction with carbon form a metal carbide layer. Niobium is an attractive metal because of its ability to form chemically stable films of niobium carbides (Nb_xC_y) on diamond surfaces. These films have exceptional characteristics, such as good superconductivity, high melting point, and remarkable mechanical hardness [12–15] and can be used in a variety of industries [16–20]. For example, smooth and crack-free NbC coatings with thicknesses in the range of 8.75–17.10 μm, roughness of 1.29–2.28 μm, and hardness of 1558–2286 HV_{0.1} were obtained on the surface of AISI D3 steel under different temperature conditions [21]. Such coatings can improve the wear resistance and corrosion resistance of steel.

Despite the existence of several production methods, synthesizing NbC materials and films remains a challenging task due to the exceptionally high melting point of Nb at 2751 K. Niobium carbide films can be obtained by reactive magnetron sputtering [22–24], thermoreactive diffusion [25], chemical solution and polymer deposition [26].

* Corresponding author.

E-mail address: j.bondareva@skoltech.ru (J.V. Bondareva).

However, the existence of several production methods, the synthesis of niobium carbide films remains a challenge because of the exceptionally high melting point of Nb (2751 K) and significant deviations from the stoichiometric composition. The lack or excess of carbon in the synthetic mixture led to the presence of carbon vacancies or excess of amorphous carbon, correspondingly, which worsen the various properties of such carbides [27,28]. Therefore, reaching the stoichiometric perfection of NbC is an important task for improving the conductive properties [29,30] of the resulting films.

In this work, we have developed a simple method for obtaining adhesive-strong films of stoichiometrically perfect NbC on the diamond surface. Niobium was deposited onto a diamond surface by magnetron sputtering and annealed in a vacuum to form NbC. The purpose of this work is to investigate the conditions of obtaining adhesive-strong, homogeneous and island-like layers of stoichiometrically perfect NbC on diamond, as well as to study their properties. Such films on diamonds are promising in various fields of science and technology especially for single photon detectors [31].

2. Experimental

2.1. Films fabrication

Polished plates made of single-crystal natural diamond were used for Nb sputtering. First, the plates were subjected to high-temperature annealing (1600 °C) for an hour in a vacuum graphite furnace (residual gas pressure $\sim 2 \times 10^{-5}$ Torr). Then the samples were cleaned in a mixture of $H_2SO_4 + K_2Cr_2O_7$ at 150 °C and washed several times in boiling distilled water [32]. The deposition of Nb was carried out by magnetron sputtering at direct current with rate 0.5–1 nm/sec. The sputtering target was made of Nb (99.999%) with a diameter 6.8 cm. The deposition was carried out in an argon atmosphere (99.999%) at a pressure of 5×10^{-2} Torr. Nb was deposited at two temperatures: room temperature and 650 °C. The thicknesses of the deposited Nb films ranged from 8 nm to 2 μ m. To form niobium carbide films, diamond samples with Nb films were annealed in a vacuum (residual gas pressure $\sim 2 \times 10^{-5}$ Torr) graphite furnace at temperatures from 800 to 1600 °C for 1 h.

2.2. Morphology characterization

The morphology was studied by scanning electron microscopy (SEM) on JEOL JSM7001F instruments with energy of 30 keV. The elemental composition was controlled by the EDS method using the same microscope using the INCA Energy spectrometer. For the detailed analysis the transmission electron microscopy (TEM) JEM 2100 F (UHR/Cs) equipped with JEOL JED2300 series EDX was carried out. Sample preparation for TEM study was cut by electron gun with deposited Pt and Au layers. The thermal analyzer STA 449 F3 Jupiter (NETZSCH) with a heating speed of 30 K/min up to 1300 °C in the Ar atmosphere was used for the registration of the phase transition. For thermal analysis the Nb and C powder was used. The structural characteristics of the films were studied at room temperature on a Panalytical X'Pert Pro MRD Extended X-ray diffractometer with a parabolic X-ray mirror as a primary monochromator at Cu K α 1 wavelength. The diffractograms were recorded with a parabolic X-ray mirror as a primary monochromator with a deviation from the maximum of C (220) peak by $\omega = -0.5^\circ$ in order not to veil weak peaks of NbC layer by strong diamond reflexes and not to miss the possible preferential orientation of crystallites in the layer. For surface roughness analysis of the samples NbC/diamond we used the atomic force microscope (AFM) NT-MDT (INTEGRA series) setup in classical semi contact mode and high accuracy composite probe (HA_NC/50) with resonant frequency 237 kHz. The scanning speed of the sample surface was 0.5 Hz. Before surface examination the samples were placed for 30 min in an ultrasonic bath with warm isopropanol to remove possible surface contaminants. After isopropanol, the samples

were dried out with compressed nitrogen.

2.3. DC transport measurements

The measurement of dependence of resistivity on temperature $R(T)$ was performed on a specialized flat holder where thermometer and a sample were set. When measuring $R(T)$, the film was not patterned. Electrical contact to the film surface is carried out by pressing through the indium interlayer. Resistance measurements were carried out according to the four-probe technique. Either a Keithley 2400 multimeter or a LakeShore 370 resistance bridge was used to measure resistance. To measure the temperature, a calibrated LakeShore DT-470 diode was used, which was controlled by the LakeShore Temperature Controller 331. For measurements in the temperature range 300 K - 1.7 K, the holder was placed in a cryogenic case with vacuum walls, which then was immersed in a Dewar vessel with liquid helium. In this experiment, critical temperature T_c corresponds to the temperature of 50% sample resistance of normal state. To study the influence of a magnetic field on the resistance, a superconducting Nb₃Sn solenoid, immersed in a Dewar vessel with liquid helium, was used. A Delta Electronics power supply (60 A, 4 T) was used to generate the magnetic field. In experiments involving a magnetic field, the sample was placed in the center of the solenoid, perpendicular to the lines of the magnetic field. A calibrated Allen Bradley carbon resistance thermometer that is not sensitive to magnetic fields was used. The critical current density determined from the results of measurements of the critical current at some fixed temperature in a patterned sample: $j_c = I_c/(w^*d)$, where I_c is the critical current, d is the film thickness and w is the sample width. The sample is patterned in a rectangular strip. The value of the critical current is determined from the current-voltage (I-V) dependence of the sample. The I-V measurements are carried out using the two-point probe technique. The bias is carried out in the voltage source mode ($r < < RL$, where r is the internal resistance of the source and RL is the load resistance), when the voltage on the sample is controlled and the current value is measured. The measured critical current I_c is determined as the current cutoff point, which is the maximum current point in the I-V dependence. A Keithley 2400 multimeter is used to measure the current-voltage characteristics.

2.4. Computational details

Calculations of thermodynamic stability of known crystal structures in NbC system were performed by using density functional theory (DFT) [33,34] as implemented in VASP package [35–37], allowing the accurate structure relaxation and total energy computations within the generalized gradient approximation (the Perdew–Burke–Ernzerhof functional) [38] and the projector augmented wave method [39,40].

3. Results and discussion

To determine the processes that occur during annealing of Nb, a differential thermal analysis of a mixture of graphite and niobium powders was performed. The results of the study are shown in Fig. 1a, which displays the peak around 850 °C corresponds to the formation of carbides [41]. Presumably, this peak belongs to the phase transformation from Nb and C to Nb₂C. The energy formation of Nb₂C from elemental atoms at 0 K is equal – 0.532 eV/atom. This result is proved by XRD study.

The film deposited on diamond at 650 °C has the polycrystalline structures without prominent peaks Fig. 1b. A weak peak at 33.3 degrees appears after annealing at 800 °C which represents the (210) Nb₂C reflex, which correlates with thermal analysis. After annealing at 1000 and 1100 °C, Nb₂C and NbC phase reflexes are visible. Annealing at 1200 °C leads to the complete disappearance of Nb and Nb₂C reflexes – only strong NbC reflexes are visible, which was also confirmed by the thermal analysis. However, the transformation of Nb₂C to NbC is not seen in the

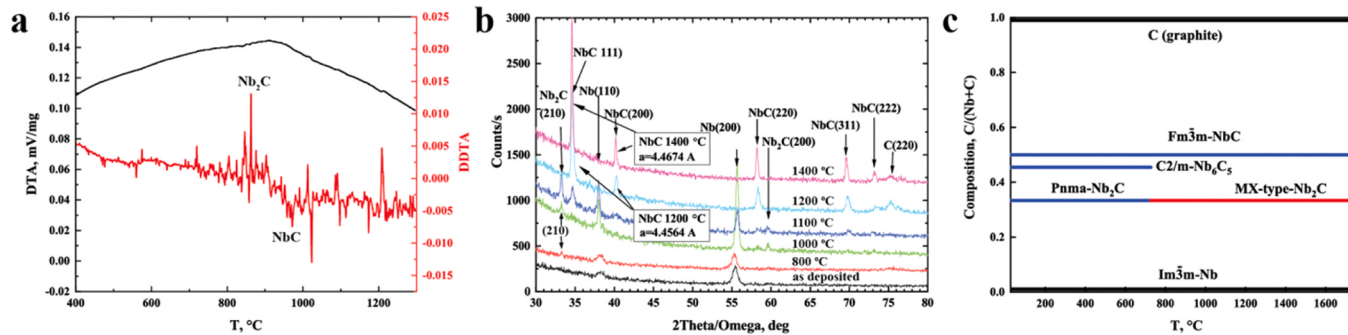


Fig. 1. (a) Differential thermal analysis of Nb and C powder mixture. (b) XRD spectra of the Nb films on the diamond at different stages of annealing. (c) Calculated composition-temperature phase diagram of Nb-C compounds.

DTA and DDTA curves. The transformation energy is much lower than for the formation of Nb₂C and equal to -0.16 eV/atom.

For the Nb-C system we have calculated the composition-temperature phase diagram using the harmonic approximation as shown in Fig. 1c. As one can see several compounds may exist at different temperatures. Cubic NbC becomes thermodynamically stable

at temperature higher than 27 °C, while Nb₆C₅ is stable at low temperature below 723 °C. Orthorhombic Nb₂C is stable from 0 to 727 °C while at higher temperatures it undergoes phase transition to its MX-type counterparts Nb_{1.33}C or Nb₄C₃, which are stable until 1727 °C [42].

We have plotted the dependence of the Nb_xC_y lattice parameter on the Nb:C ratio, as shown in Fig. 2a, b. It can be observed that lattice

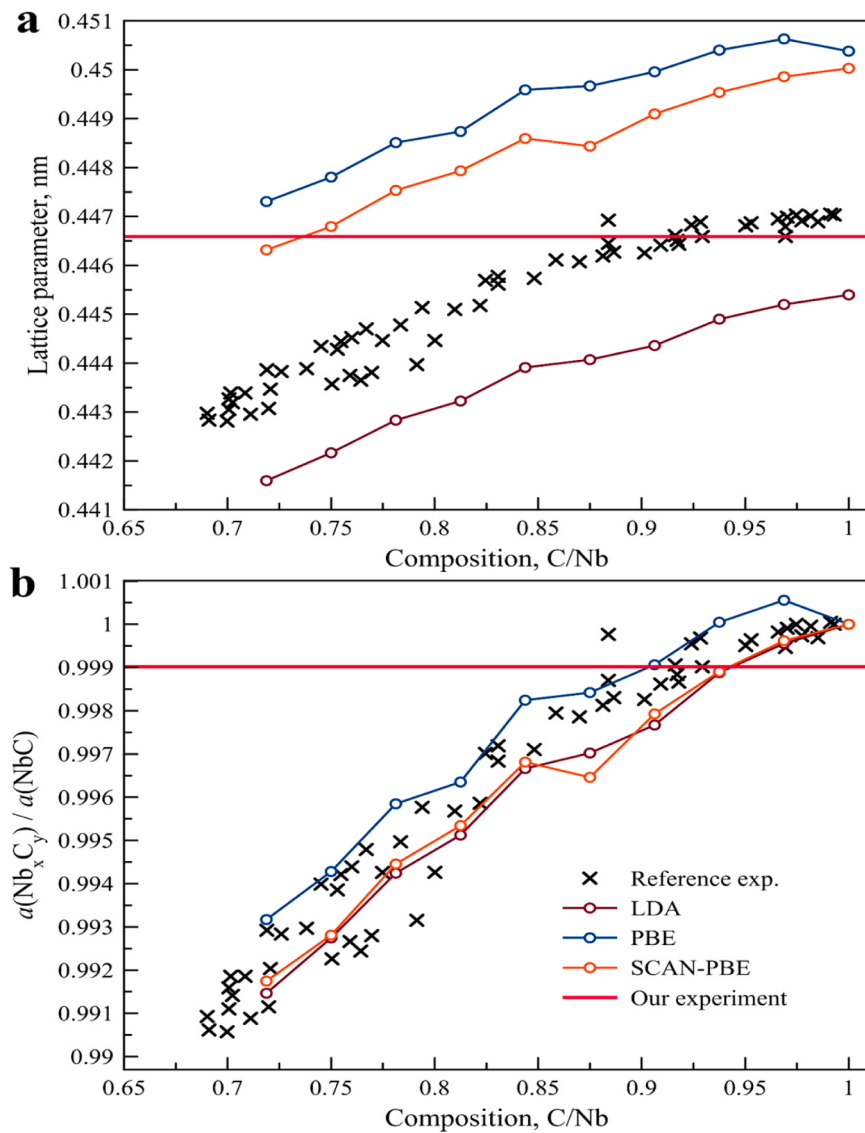


Fig. 2. Dependence of (a) lattice parameter on composition and (b) relative lattice parameter of Nb_xC_y with respect to Nb:C= 1:1 depending on the composition [43].

parameters monotonically increase with an increasing Nb:C ratio from 0.7 to 1 (Fig. 2a). We have also computed the relative lattice parameters as ratio of Nb_xC_y lattice parameters to NbC as shown in Fig. 2b. It should be noted that the measured lattice parameter of the obtained NbC sample is 0.999 out of that for NbC. Based on this comparison and Fig. 2a, b we can conclude about the Nb:C ratio in our sample which is close to 0.9.

Films deposited at room temperature become island-like after annealing. According to the phase diagram, niobium carbide can form at a temperature of about 600 °C [15]. Deposition of niobium at 650 °C results in good adhesion and the formation of solid 1 μm thick Nb nanocrystalline films on (110) diamond with the size of Nb crystallites reaches 100 nm, Fig. 3. The diamond surface appears to be corroded in the place where the film was located after the chemical etching of film. This indicates the dissolution of carbon from the surface layers of the diamond in the niobium film and its participation in the formation of niobium carbides. As a result of annealing at temperatures of 800–1600 °C thick films (up to 2.5 μm) remain continuous.

X-ray diffraction shows the presence of the Nb_2C phase at annealing temperatures 1000–1100 °C. In this range, SEM images reveal grains of two completely different types (they are denoted as "1-yellow" and "2-blue"). Grains of the "1" phase sized 100–200 nm have a very developed surface of skeletal type. Grains of the "2" phase look like liquid layers and droplets up to 1 μm. In the temperature range of 1000–1100 °C the Nb_2C phase can exist in two crystal modifications - monoclinic (mp-569989) and orthorhombic (mp-2318) [44]. Calculated composition-temperature phase diagram for Nb-C system supports the probability of formation of Nb_2C at high temperatures. According to previous research [15,45,46] the Nb_6C_5 ($NbC_{0.83}$) with monoclinic or trigonal crystal lattice is stable up to 1050 °C or even 1320 °C [42,47]. It gives the same reflexes [46,48] as NbC, only with a slightly different ratio of intensities, due to the fact that it is actually a cubic structure of NbC with almost the same interatomic distance, only with an ordered arrangement of carbon vacancies. In Fig. 3 "yellow" phase can be attributed to Nb_2C . After annealing at 1200 °C, there are only NbC reflexes, but the "blue" phase is detectable in the SEM image. Absence of the "blue" phase in XRD peaks can be explained by low concentration or by amorphous nature. We can assume that it is the Nb_6C_5 phase with the same reflexes. According to SEM and X-ray diffraction data, Nb crystals completely disappear at an annealing temperature of 1200 °C. The temperature range of Nb_2C phase existence is 1000–1100 °C. Only NbC crystallites are detected starting from 1200 °C according to SEM, X-ray

analysis. This means that annealing at 1200 °C is sufficient to form a continuous film of pure NbC. After annealing at 1400 °C, the intensity and the FWHM of all NbC diffraction peaks increases remarkably. Together with the SEM patterns, this suggests an improvement in the crystalline perfection of the film and an increase in the size of crystallites due to solid-phase recrystallization. The NbC grains are formed by tabular-shaped layers a few tens of nanometers thick. Annealing at 1600 °C leads to insignificant changes in the morphology and X-ray diffraction of the NbC film. According to EDX data, films after annealing do not contain any impurities, including oxygen (sensitivity not worse than 0.1%). NbC films have high adhesion on the diamond and at thickness up to 2.5 μm remain integral even after annealing at 1600 °C. To investigate the roughness of the films, niobium of various thicknesses was deposited at a temperature of 650 °C. After the deposition of the films, samples were annealed at a temperature of 1400 °C. For 8 nm film the root mean square roughness (S_q) is approximately 2 nm Fig. 4a,b. Subsequently, with an increase in thickness to 100 nm, a significant rise in roughness to 20 nm is observed Fig. 4c. However, from 100 to 1500 nm, the roughness remains relatively constant Fig. 4d.

Interface between the diamond and NbC is shown in Fig. 5. The 100 nm Nb film annealed at 1400 °C were chosen for the study. It can be seen in Fig. 5a that the boundary between diamond and the formed niobium carbide is flat. The EDX analysis shows in Fig. 5b, a uniform distribution of elements within the sample can be observed. Fig. 5c depicts a high-resolution TEM image of NbC, showing a film formed of nanocrystals of about ten nanometers.

Sample cooling after annealing leads to the formation of tetragonal deformation due to tensile stress. According to X-ray diffraction data upon (2q-w)-scanning with a third crystal analyzer on reflexes (111) and (200), the crystal lattice parameter in the NbC film in the normal direction after annealing at 1400 °C is 4.4618 Å, in the film plane is 4.4930 Å. Taking into account the elastic properties of NbC [15], this corresponds to mechanical tensile stress in the film plane of ~2 GPa. To test the uniformity of the films the thickness was decreased to a few nanometers. The Nb films deposited on diamond at 650 °C remain continuous. Annealing of such samples at 1400 °C made it possible to obtain adhesive-strong NbC films on diamond with a thickness from 30 nm (± 5 nm). The size of NbC crystallites in thin films is approximately equal to the film thickness.

Niobium carbide films annealed at more than 1400 °C were investigated for superconductivity. The critical temperature T_c at zero magnetic field corresponds to ~12.4 K. With the introduction of a magnetic

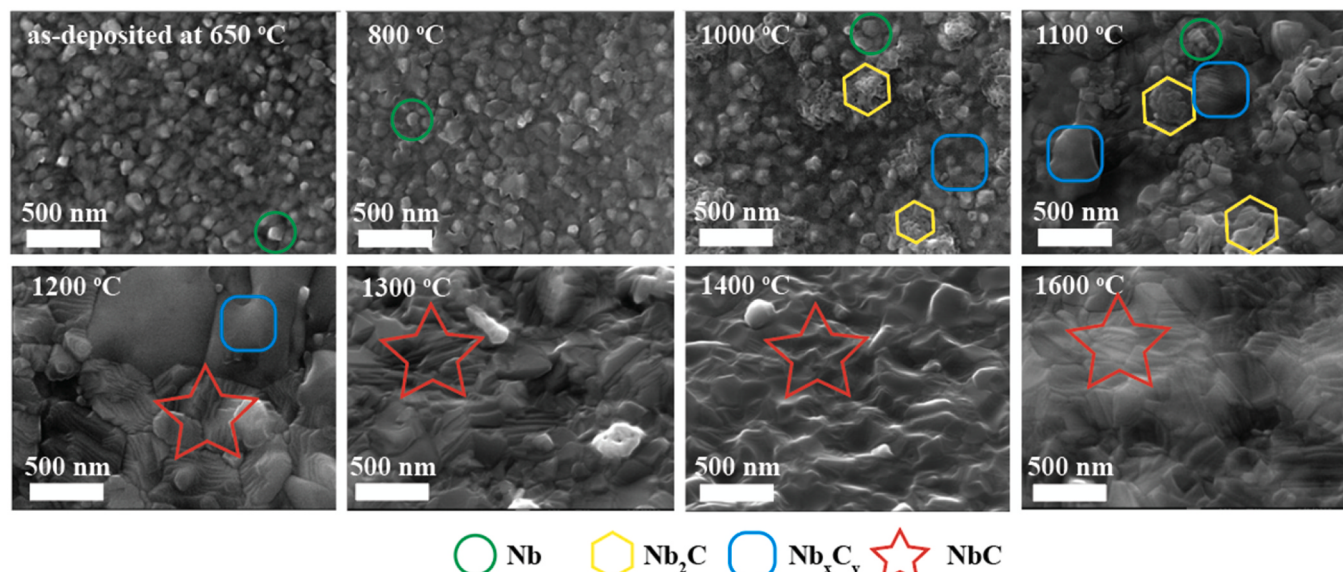


Fig. 3. SEM images of 1 μm Nb films deposited at 650 °C and annealing at different temperatures.

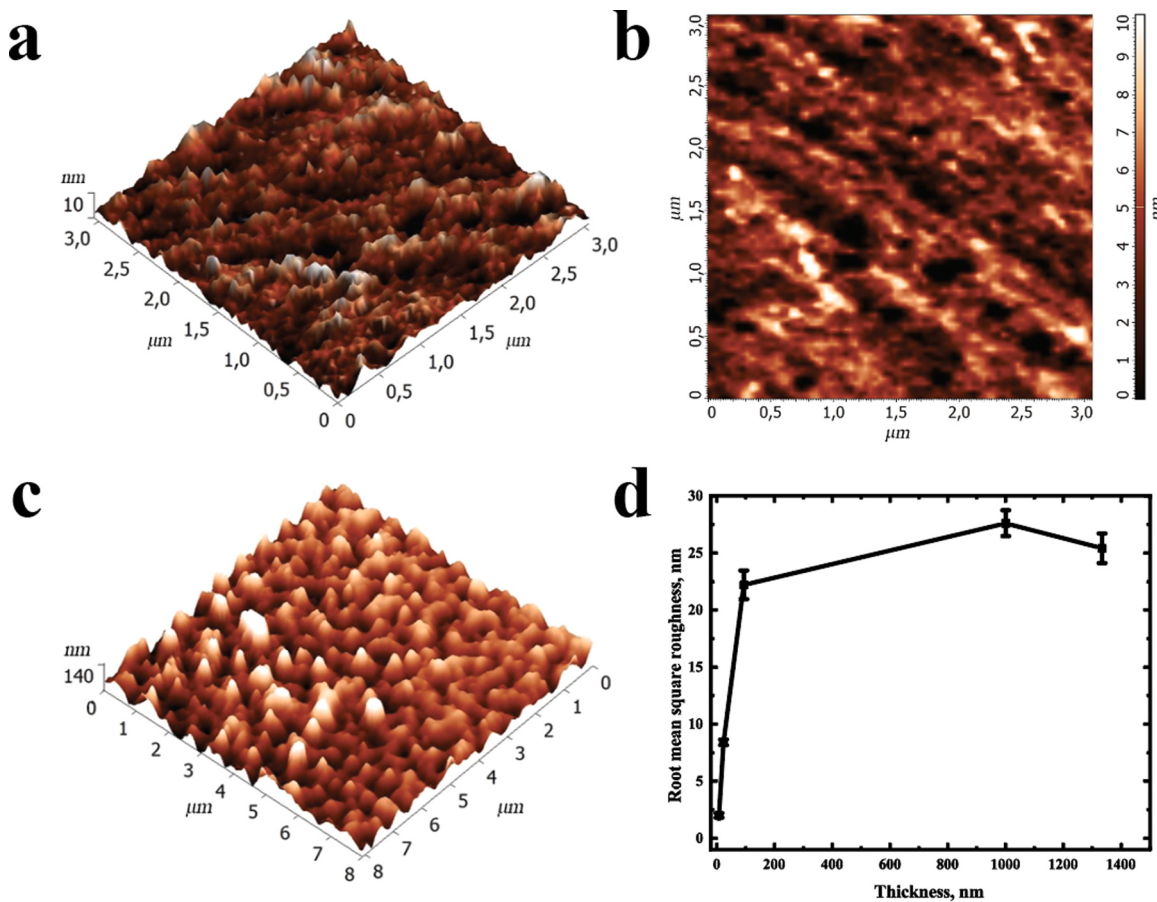


Fig. 4. (a) – (b) Surface of sample with thickness 8 nm, (c) surface of sample with thickness of NbC 1400 nm, (d) evolution of roughness of the films annealed at 1400 °C.

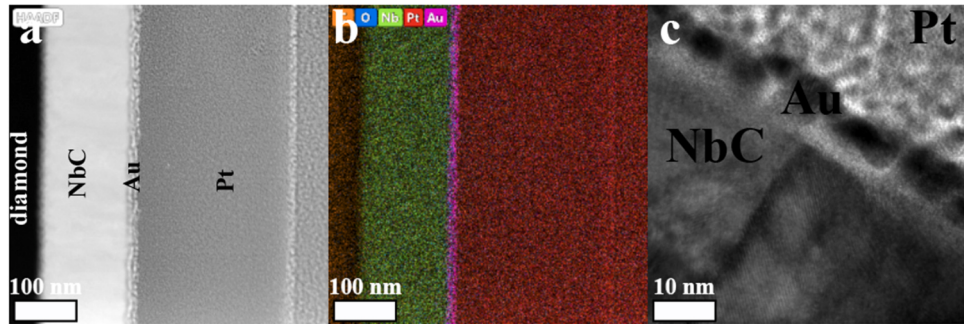


Fig. 5. (a) TEM images of produced sample, (b) Element distribution in the film, (c) high resolution TEM images of the NbC.

field perpendicular to the plane of the sample, a shift of the $R(T)$ curves towards low temperatures is observed (shown in Fig. 6a). From the experimental dependences of $R(T)$ at different magnetic fields, one can estimate: the second critical field, the coherence length and the electron diffusion coefficient – $B_{c2}(0) = -0.69 T_c$ (dB_{c2}/dT), $\xi_{GL}^2(0) = \pi\hbar D/(8k_B T_c)$ and $D = -4k_B/(\pi e)$ (dB_{c2}/dT) $^{-1}$, respectively. We considered the temperature at which the resistance is $R = 0.5R_N$, where R_N is the resistance over the resistive transition, as the temperature corresponding to the value of the critical field B_{c2} at a given temperature. The study of the experimental curves gives the value $dB_{c2}/dT = -0.156$ T/K (Fig. 6b), which gives the following estimates for the second critical field, the coherence length and the diffusion coefficient – ~ 1.34 T, ~ 13 nm and 7 cm 2 /s, respectively. Fig. 6c presents the dc current-voltage characteristics for the patterned sample with a length L

$= 1$ mm, a width $w = 1.13$ mm and the thickness $d = 200$ nm. We should note that all current-voltage characteristics deviate from the zero-resistance curve even before reaching the maximum critical current through the sample. This is due to the measurement of the sample in a two-point probe configuration and, accordingly, the contribution of the resistance of the wires from the measuring system. In our case, this additional resistance of the wires does not exceed 15% of the resistance of the sample in the normal state. Also, the sample and the measuring wires are connected in series, so the additional resistance does not affect the accuracy of determining the critical current. The estimated critical current density at $T = 6.7$ K is 2.87×10^5 A/cm 2 . The measured critical current density at different temperatures generally follows the behavior predicted by the Ginzburg-Landau (GL) theory [49] $j_c(t) \sim (1-t^2)^{3/2}(1+t^2)^{1/2}$, where $t = T/T_c$ is the reduced temperature (see the

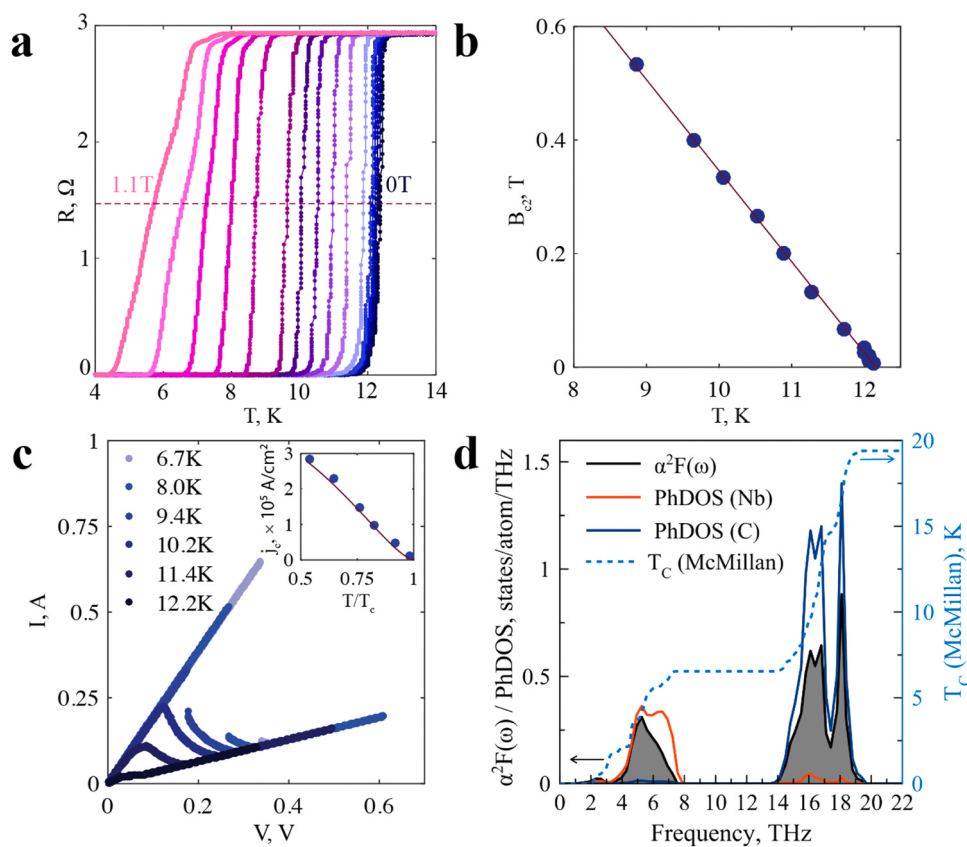


Fig. 6. (a) Temperature dependences of the resistance at different magnetic fields. (b) The temperature dependence of the second critical magnetic field $B_{c2}(T)$. (c) The current-voltage dependencies at different bath temperatures. The inset: the temperature dependence on the critical current density. The solid lines show the T -dependence in the frame of the GL theory. (d) Eliashberg spectral $\alpha^2F(\omega)$ function (shaded area), phonon density of states projected on Nb (red) and carbon (blue), and integral critical temperature (blue dashed line).

inset in Fig. 6c). From the fit to the data we conclude a critical current density at zero temperature $j_c(0) = 4 \times 10^5 \text{ A}/\text{cm}^2$. We compared the measured values I_c with the depairing current of dirty superconductors using the formula [50]:

$$I_{\text{dep}}(0) = 0.74(w[\Delta(0)]^{3/2})/(e R_s(\hbar D)^{1/2})$$

$\Delta(0)$ is the superconducting energy gap at 0 K, e is the electron charge, R_s is the resistance per square, D is the diffusivity. Using this formula we found that $j_{\text{dep}}(0) = I_{\text{dep}}(0)/(w \cdot d) \sim 10^7 \text{ A}/\text{cm}^2$. This difference may be explained by the presence of various defects in the film structure, which allow the vortex lattice to become anchored. We have also studied electron-phonon coupling in NbC. First, we performed the calculations of phonon density of states projected to each atomic type as shown in Fig. 6d. Superconducting properties of NbC were studied by using DFPT and the Eliashberg spectral function was plotted as shown by the shaded area in Fig. 6d. One can see that light carbon atoms make a greater contribution to superconductivity compared to Nb (dashed line in Fig. 6d). The critical superconducting temperature estimated by McMillan formula is equal to 19.4 K.

4. Conclusion

In this paper, we focus on solving the problem of diamond metallization by creating adhesive-strong films of stoichiometrically perfect NbC on its surface. Niobium was deposited on the diamond surface by magnetron sputtering and annealed in vacuum to form NbC at different temperatures. Such films on diamond are promising in various fields of science and technology, especially for single-photon detectors. During the work, we investigated how the annealing temperature affects the distribution of phases in a niobium carbide film. It was found that at an

annealing temperature of 1300 °C a uniform film of stoichiometrically perfect niobium carbide is formed on the diamond surface. We have obtained a niobium carbide film several nanometers thick, which exhibits superconducting behavior up to 12.4 K. The lattice parameter of the film is 4.4659 Å, which is close to the maximum value for the lattice parameters of NbC. According to DFT calculations, the critical superconducting temperature is equal to 19.4 K.

Funding

This work was financially supported by the Russian Science Foundation. Study the properties of materials was carried out within the framework of the Russian Science Foundation project # 22-73-10198, <https://www.rscf.ru/en/project/22-73-10198/>, study of superconductivity was conducted in within the framework of the Russian Science Foundation project # 21-72-10117 <https://www.rscf.ru/en/project/21-72-10117/>.

CRediT authorship contribution statement

R.A. Khmelnitsky: Conceptualization (equal), Formal analysis (equal), Investigation (lead); Writing – review & editing (equal), Supervision (lead) **V.P. Martovitsky:** Conceptualization (equal), Investigation (lead), Visualization (lead); **J.V. Bondareva:** Visualization (equal); Writing – original draft (equal); Writing – review & editing (lead). **A.I. Kolbatova:** Data curation (equal), Investigation (lead), Methodology (equal); **N.A. Titova:** Data curation (equal), Investigation (lead), Methodology (equal); **G.N. Goltzman:** Data curation (equal), Methodology (equal), Formal analysis (equal); **F.S. Fedorov:** Data curation (equal), Formal analysis (equal), Methodology (equal); **A.V.**

Egorov: Data curation (equal); Formal analysis (equal); **N.A. Matsokin, A.G. Kvashnin:** Visualization (lead), Data curation (equal); Formal analysis (equal); **D.G. Kvashnin:** Visualization (lead), Data curation (equal); Formal analysis (equal); **S.A. Evlashin:** Investigation (lead), Writing – review & editing (equal), Supervision (lead).

Declaration of Competing Interest

The authors declare that they have no known competing financial interests or personal relationships that could have appeared to influence the work reported in this paper.

Data Availability

No data was used for the research described in the article.

Acknowledgements

Samples preparation was made in Advanced Imaging Core Facility of Skoltech.

References

- [1] C.J.H. Wort, R.S. Balmer, Diamond as an electronic material, Mater. Today 11 (1) (2008) 22–28.
- [2] I. Aharonovich, A.D. Greentree, S. Prawer, Diamond photonics, Nat. Photon 5 (7) (2011) 397–405.
- [3] C.A. Brookes, E.J. Brookes, Diamond in perspective: a review of mechanical properties of natural diamond, Diam. Relat. Mater. 1 (1) (1991) 13–17.
- [4] Yu V. Pleskov, Electrochemistry of diamond: a review, Russ. J. Electrochim. 38 (12) (2002) 1275–1291.
- [5] A.V. Inyushkin, A.N. Taldenkov, V.G. Raichenko, A.P. Bolshakov, A.V. Koliadin, A. N. Katrusha, Thermal conductivity of high purity synthetic single crystal diamonds, Phys. Rev. B 97 (14) (2018), 144305.
- [6] S. Shikata, Single crystal diamond wafers for high power electronics, Diam. Relat. Mater. 65 (2016) 168–175.
- [7] C. Artini, M.L. Muolo, A. Passerini, Diamond–metal interfaces in cutting tools: a review, J. Mater. Sci. 47 (7) (2012) 3252–3264.
- [8] J. Nakanishi, et al., Formation of ohmic contacts to p-type diamond using carbide forming metals, J. Appl. Phys. 76 (4) (1994) 2293–2298.
- [9] C. Monachon, L. Weber, Thermal boundary conductance between refractory metal carbides and diamond, Acta Mater. 73 (2014) 337–346.
- [10] “Handbook of Diamond Technology | Book | Scientific.Net,” (n.d.).
- [11] D.A. Evans, O.R. Roberts, G.T. Williams, A.R. Veary-Roberts, F. Bain, S. Evans, D. P. Langstaff, D.J. Twitchen, Diamond–metal contacts: interface barriers and real-time characterization, J. Phys. Condens Matter 21 (36) (2009), 364223.
- [12] M. Woydt, H. Mohrbacher, The use of niobium carbide (NbC) as cutting tools and for wear resistant tribosystems, Int. J. Refract. Met. Hard Mater. 49 (2015) 212–218.
- [13] W.S. Williams, The thermal conductivity of metallic ceramics, JOM 50 (6) (1998) 62–66.
- [14] R.F. Brenton, C.R. Saunders, C.P. Kempfer, Elastic properties and thermal expansion of niobium mono-carbide to high temperatures, J. Less Common Met. 19 (3) (1969) 273–278.
- [15] M.G.D.V. Cuppari, S.F. Santos, Physical properties of the NbC carbide, Metals 6 (10) (2016) 250.
- [16] M. Woydt, S. Huang, J. Vleugels, H. Mohrbacher, E. Cannizza, Potentials of niobium carbide (NbC) as cutting tools and for wear protection, Int. J. Refract. Met. Hard Mater. 72 (2018) 380–387.
- [17] S.T. Oyama, The Chemistry of Transition Metal Carbides and Nitrides, Springer Netherlands, Dordrecht, 1996.
- [18] A. Tolosa, B. Krüner, S. Fleischmann, N. Jäckel, M. Zeiger, M. Aslan, I. Grobelsek, V. Presser, Niobium carbide nanofibers as a versatile precursor for high power supercapacitor and high energy battery electrodes, J. Mater. Chem. A 4 (41) (2016) 16003–16016.
- [19] L. Lan, X. Fan, Y. Gao, G. Li, Q. Hao, T. Qiu, Plasmonic metal carbide SERS chips, J. Mater. Chem. C. 8 (41) (2020) 14523–14530.
- [20] C. Liu, J. Zhou, X. Li, Z. Fang, R. Sun, G. Yang, W. Hou, Surface modification and in situ carbon intercalation of two-dimensional niobium carbide as promising electrode materials for potassium-ion batteries, Chem. Eng. J. 431 (2022), 133838.
- [21] A. Günen, H.H. Açıkgöz, M. Keddam, İ.H. Karahan, Characterizations and kinetics of refractory niobium carbide coatings on AISI D3 steel, J. Mater. Eng. Perform. 32 (19) (2023) 8972–8980.
- [22] N. Nedfors, O. Tengstrand, E. Lewin, A. Furlan, P. Eklund, L. Hultman, U. Jansson, Structural, mechanical and electrical-contact properties of nanocrystalline-NbC/amorphous-C coatings deposited by magnetron sputtering, Surf. Coat. Technol. 206 (2) (2011) 354–359.
- [23] M.Y. Liao, Y. Gotoh, H. Tsuji, J. Ishikawa, Compound-target sputtering for niobium carbide thin-film deposition, J. Vacuum Sci. Technol. B: Microelectron. Nanomet. Struct. Proc. Meas. Phenom. 22 (5) (2004) L24–L27.
- [24] K. Zhang, M. Wen, G. Cheng, X. Li, Q.N. Meng, J.S. Lian, W.T. Zheng, Reactive magnetron sputtering deposition and characterization of niobium carbide films, Vacuum 99 (2014) 233–241.
- [25] A. Günen, H.H. Açıkgöz, İ.H. Karahan, Niobium carbide coatings grown on cold work tool steel AISI D3 by thermomechanical processing: characterization, wear and corrosion behaviors, Prot. Met. Phys. Chem. Surf. 59 (4) (2023) 648–670.
- [26] G. Zou, H. Luo, Y. Zhang, J. Xiong, Q. Wei, M. Zhuo, J. Zhai, H. Wang, D. Williams, N. Li, E. Bauer, X. Zhang, T.M. McCleskey, Y. Li, A.K. Burrell, Q.X. Jia, A chemical solution approach for superconducting and hard epitaxial NbC film, Chem. Commun. 46 (41) (2010) 7837–7839.
- [27] X.-X. Yu, G.B. Thompson, C.R. Weinberger, Influence of carbon vacancy formation on the elastic constants and hardening mechanisms in transition metal carbides, J. Eur. Ceram. Soc. 35 (1) (2015) 95–103.
- [28] L.G. Radosevich, W.S. Williams, Phonon scattering by conduction electrons and by lattice vacancies in carbides of the transition metals, Phys. Rev. 181 (3) (1969) 1110–1117.
- [29] Y. Ishizawa, S. Otani, H. Nozaki, T. Tanaka, Carbon-vacancy concentration dependencies of electrical properties of NbC_x single crystals, J. Phys.: Condens. Matter 4 (44) (1992) 8593–8598.
- [30] A.L. Giorgi, E.G. Szklarz, E.K. Storms, A.L. Bowman, B.T. Matthias, Effect of composition on the superconducting transition temperature of tantalum carbide and niobium carbide, Phys. Rev. 125 (3) (1962) 837–838.
- [31] K. Y. S. M. S. A. K. S. M. K. A. Korneev, G. Chulkova, G. Goltsman, Comparison of hot spot formation in NbC and NbN single photon detectors, IEEE Trans. Appl. Supercond. 26 (3) (2016) 1–4.
- [32] R.A. Khmelnitsky, S.A. Evlashin, V.P. Martovitsky, P.V. Pastchenko, S.A. Dagesian, A.A. Alekseev, N.V. Suetin, A.A. Gippius, Heteroepitaxy of Ni-based alloys on diamond, Cryst. Growth Des. 16 (3) (2016) 1420–1427.
- [33] P. Hohenberg, W. Kohn, Inhomogeneous electron gas, Phys. Rev. 136 (3B) (1964) B864–B871.
- [34] W. Kohn, L.J. Sham, Self-consistent equations including exchange and correlation effects, Phys. Rev. 140 (4A) (1965) A1133–A1138.
- [35] G. Kresse, J. Hafner, Ab initio molecular dynamics for liquid metals, Phys. Rev. B 47 (14) (1993) 558–561.
- [36] G. Kresse, J. Hafner, Ab initio molecular-dynamics simulation of the liquid-metal-amorphous-semiconductor transition in germanium, Phys. Rev. B 49 (20) (1994) 14251–14269.
- [37] G. Kresse, J. Furthmüller, Efficient iterative schemes for ab initio total-energy calculations using a plane-wave basis set, Phys. Rev. B 54 (16) (1996) 11169–11186.
- [38] J.P. Perdew, K. Burke, M. Ernzerhof, Generalized gradient approximation made simple, Phys. Rev. Lett. 77 (18) (1996) 3865–3868.
- [39] P.E. Blöchl, Projector augmented-wave method, Phys. Rev. B 50 (24) (1994) 17953–17979.
- [40] G. Kresse, D. Joubert, From ultrasoft pseudopotentials to the projector augmented-wave method, Phys. Rev. B 59 (3) (1999) 1758–1775.
- [41] Y.O. Kuzminova, E.A. Kudryavtsev, J.-K. Han, M. Kawasaki, S.A. Evlashin, Phase and structural changes during heat treatment of additive manufactured CrFeCoNi high-entropy alloy, J. Alloy. Compd. 889 (2021), 161495.
- [42] C.R. Weinberger, G.B. Thompson, Review of phase stability in the group IVB and VB transition-metal carbides, J. Am. Ceram. Soc. 101 (10) (2018) 4401–4424.
- [43] C.P. Kempfer, E.K. Storms, R.J. Fries, Lattice dimensions of NbC as a function of stoichiometry, J. Chem. Phys. 33 (6) (2004) 1873–1874.
- [44] K. Yvon, H. Nowotny, R. Kieffer, Die kristallstruktur der subcarbide von Übergangsmetallen, Mon. für Chem. 98 (1) (1967) 34–44.
- [45] I.L. Shabalin, in: I.L. Shabalin (Ed.), Ultra-High Temperature Materials II: Refractory Carbides I (Ta, Hf, Nb and Zr Carbides), Springer Netherlands, Dordrecht, 2019, pp. 249–422.
- [46] L. Wu, Y. Wang, Z. Yan, J. Zhang, F. Xiao, B. Liao, The phase stability and mechanical properties of Nb–C system: using first-principles calculations and nano-indentation, J. Alloy. Compd. 561 (2013) 220–227.
- [47] A.I. Gusev, A.A. Rempel, Phase diagrams of metal–carbon and metal–nitrogen systems and ordering in strongly nonstoichiometric carbides and nitrides, Phys. Status Solidi (a) 163 (2) (1997) 273–304.
- [48] A.I. Gusev, A.A. Rempel, Order-disorder phase transition channel in niobium carbide, Phys. Status Solidi (a) 93 (1) (1986) 71–80.
- [49] W.J. Skocpol, M.R. Beasley, M. Tinkham, Self-heating hotspots in superconducting thin-film microbridges, J. Appl. Phys. 45 (9) (2003) 4054–4066.
- [50] Yu.P. Korneeva, D.Yu Vodolazov, A.V. Semenov, I.N. Florya, N. Simonov, E. Baeva, A.A. Korneev, G.N. Goltsman, T.M. Klapwijk, Optical single-photon detection in micrometer-scale NbN bridges, Phys. Rev. Appl. 9 (6) (2018), 064037.